Differential deposition correction of segmented glass X-ray optics

Carolyn Atkins*[a], Kiranmayee Kilaru*[b], Brian D. Ramsey[b], David M. Broadway[b], Mikhail V. Gubarev[b], Stephen L. O'Dell[b] and William W. Zhang[c]

[a]University of Alabama in Huntsville, Center for Space Plasma and Aeronomic Research, Huntsville, AL 35899, USA
[b]NASA Marshall Space Flight Center, Huntsville, AL 35812, USA
[c]NASA Goddard Space Flight Center, Greenbelt, MD 20771, USA

ABSTRACT

One of the challenges faced within the astronomical X-ray community is how to produce lightweight high angular resolution optics for a future X-ray mission capable of probing the early X-ray universe. To this end, the differential deposition project at NASA Marshall Space flight Center (MSFC) is looking to improve current X-ray optic technology by applying a corrective coating with a goal of achieving arc-second-level resolution. This paper will focus on the correction of segmented glass optics fabricated at NASA Goddard Space Flight Center (GSFC) and the paper will highlight: the design of the vacuum chamber and internal mechanics; the algorithm used to perform the correction; metrology of the glass segments; and the improvement post correction that has been achieved to date.

Keywords: Differential deposition, X-ray optics, slumped glass optics, thin film coatings

1. INTRODUCTION

To observe the early X-ray universe both high resolution and sensitivity are required within one telescope system. This is one of the primary challenges for the future of X-ray astronomy and the problem can be demonstrated by the 1999 X-ray telescope flagship missions: NASA's *Chandra X-ray Observatory*[1] and ESA's *XMM Newton*.[2] The *Chandra X-ray Observatory* achieves its impressive sub-arc second resolution through thick, accurately figured, monolithic shells; however, each of these shells is heavy and therefore the sensitivity of the telescope is limited due to only four shells being nested. In contrast, *XMM Newton* has three telescopes and each telescope has 58 nested shells offering excellent sensitivity, but the resolution is limited due to its thin electroformed nickel optics, which have higher figure error than *Chandra*'s thick monolithic mirrors.

Since 1999 smaller X-ray telescopes have been geared towards sensitivity and probing deeper in the hard X-ray range of the spectrum. For example NASA's *NuSTAR* mission,[3] launched in 2012, is the first hard X-ray observatory in orbit (previously there have been hard X-ray balloon payloads, such as *HERO*[4]) and it uses slumped glass optics with multilayers to achieve its 3keV to 79keV energy range.[5] However the optics are not designed for high resolution and the resolution of *NuSTAR* is just under a arc-minute in half power diameter (HPD). Furthermore, recent missions such as SWIFT's XRT[6] and the Russian led Spectrum Röntgen Gamma,[7] are primaily interested in high sensitivity rather than high angular resolution. More recently, in June 2014, ESA selected *ATHENA* as the second L-class mission in Cosmic Vision program, with a forseen launch in 2028.[8] *ATHENA* is a high sensitivity mission, with a proposed effective area of $2m^2$ at 1keV and an angular resolution of ~ 5 arc-sec. To achieve this performance it is thought that the optics will comprise of mirror module composed of either silicon pore optics[9] or slumped glass optics.[10] Although this resolution is a threefold improvement upon ESA's *XMM Newton*, it still a factor of 10 worse than *Chandra*.

To gain both high resolution and high sensitivity within the constraints of a launch vechicle requires a new type of optics. The optics will need to be lightweight in order to achieve the collecting area within the weight

*Further author information:
e-mail Carolyn Atkins: carolyn.atkins@uah.edu
Kiranmayee Kilaru: kiranmayee.kilaru-1@nasa.gov

Optics for EUV, X-Ray, and Gamma-Ray Astronomy VII, edited by Stephen L. O'Dell, Giovanni Pareschi,
Proc. of SPIE Vol. 9603, 96031G · © 2015 SPIE · CCC code: 0277-786X/15/$18 · doi: 10.1117/12.2189933

constraint as well as accurately figured to achieve the resolution, which should be better or at least comparable to *Chandra's* 0.5 arc-sec. Currently there is no manufacturing method that can achieve this in a single step; however, there are methods that can be applied to improve existing lightweight X-ray optics to move them from the 5-10 arc-sec domain towards the sub-arc-sec domain. Two such methods are: differential deposition,[11] which is the subject of this paper, and active X-ray optics.[12–14] Differential deposition, which is explained more thoroughly in Section 2, is the process in which a *filler* layer is added to the optical surface to fill in the optic's deformations leaving the desired optical perscription. In contrast, active optics are thin lightweight optics that are deformable through the addition of a piezoelectric material. The errors that can be corrected for via the active optics are limited to the size of the active region, therefore it is possible to combine both differential deposition and active optics so that differential deposition corrects the mid-high spatial frequencies and active optics correct the low-mid spatial frequencies.

This paper will describe the progress made in the correction of slumped glass X-ray optics, these optics build on the heritage of those used for NASA's *NuSTAR* mission and are fabricated at NASA Goddard Space Flight Center (GSFC).[15] Slumped glass optics are segmented optics that take the form of the mandrel upon which they are slumped. It is a method to quickly replicate multiple optics that are lightweight and that can be easily nested, but currently their resolution is limited to between 5-10 arc-seconds.[16] It is hoped that through the application of the differential deposition method that this resolution can be improved to approach that of an arc-second. Furthermore, differential deposition is also being applied to correct the optical deformations within the replicated NiCo optics fabricated at NASA's Marshall Space Flight Center (MSFC)[17] and this research is being presented within the paper by *Kilaru K. et al.*[18] at this conference. The two primary differences between the NiCo optics and the slumped glass optics are: 1) full revolution optics such as the NiCo optics are inherently more rigid than their segmented counterparts, and 2) the material properties are such that NiCo is stiffer and less susceptible to deformations than the glass.

2. DIFFERENTIAL DEPOSITION

The concept of differential deposition has its origins in the synchrotron field where it has been used to improve the performance of X-ray and EUV optics;[19–21] only more recently the concept has been altered to meet the needs of astronomical X-ray optics.[11, 22]

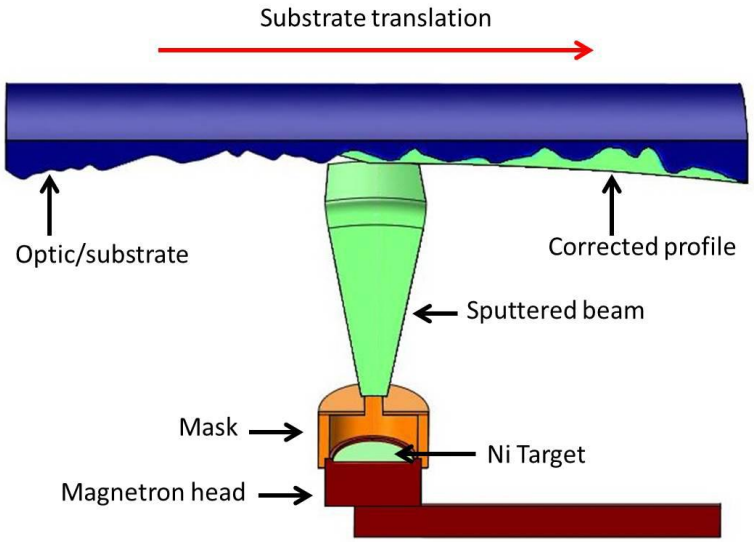

Figure 1. A concept drawing highlighting the differential deposition process. The subtrate/optic translates (and rotates) relative to the stationary magnetron head and the variable thickness profile is achieved through waiting at given points for a calculated time.

Figure 1 highlights the basic procedure for differential deposition where the optic is translated relative to a fixed sputtering source and the correction is applied by stepping the optic to distinct locations and waiting for a given dwell time. The key to a successful differential deposition correction is an accurately defined deposition profile and accurate pre/post coating metrology. By combining these two attributes through optimisation, the differential deposition correction can be achieved. Outlined within this section are: the equipment, metrology and optimisation, which are required to achieve this correction.

2.1 Equipment set-up for segmented Differential Deposition

At the end of 2013 two new vacuum chambers were constructed specifically to develop differential deposition for astronomical X-ray optics.[23] One chamber was designed for the full shell replicated NiCo optics and is described in the paper by *Kilaru K. et al. (2015)* and the second chamber was designed to coat slumped glass segmented optics,[16,24] in addition to large ∼0.5m diameter full shell optics. Within this paper the second chamber, termed the *vertical chamber*, will be described.

The vertical chamber is show in Figure 2, the chamber is approximately 1m in diameter and 1.3m in height. The chamber is divided equally into two sections and the top section is fixed to a hoist to allow access to the interior. The internal translation, ∼700 mm in range, is provided via a stepper motor mounted within a tower, the tower is not permanently fixed within the chamber and as such can be repositioned upon the rotation stage as required. The rotation stage is an annular platform with an outer diameter of 0.96m and an inner diameter of 0.62m, nested inside the rotational platform is a stationary annular platform. Both the translation and the rotation stages are fitted with optical encoders that have a resolution of $5\mu m$ and the encoder readout is used to provide feedback to ensure accurate positioning of the substrate relative to the slit in the mask.

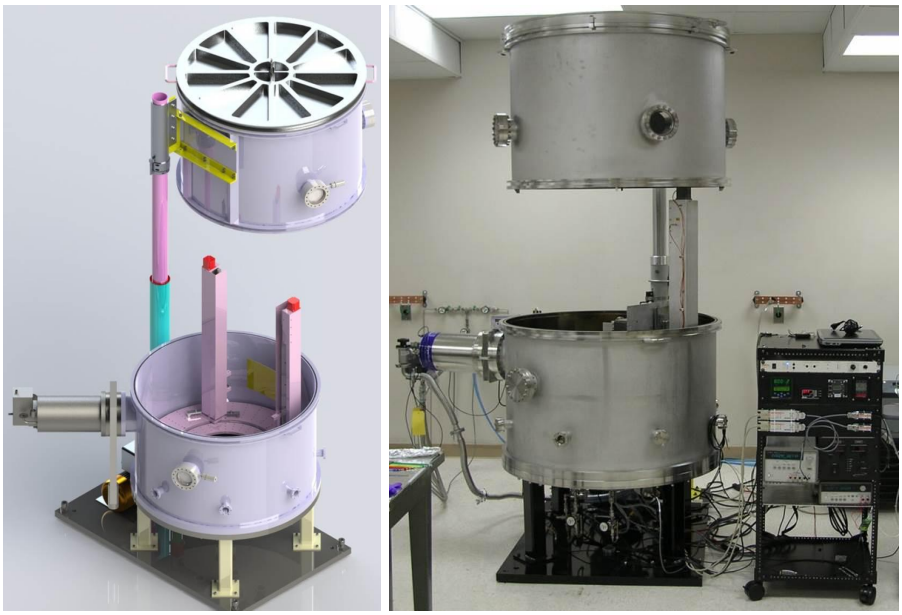

(a) (b)

Figure 2. 2(a) highlights the primary components of the vertical chamber, in particular the translation stages (the vertical towers) are shown and these are resting on the rotational stage. 2(b) displays the finished vertical chamber complete with electronics rack.

The differential deposition coating is applied using a 1 inch circular DC (direct current) magnetron sputtering head. To define the deposition profile which is used to correct the surface, a mask with a slit is placed in front of the magnetron head. The slit is located approximately 25mm from the nickel target; nickel is used as the target material primarily due to its low film stress after coating, although it also is favourable in terms of deposition rate and roughness.[11]

2.2 Metrology

The metrology for the initial experimentation upon the glass optics used a Taylor Hobson Form Talysurf with a $2\mu m$ diamond tip. The horizontal measurement range of the Form Talysurf is 200mm and using the diamond tip 0.8nm of height resolution can be obtained. To ensure no artefacts inherent within the Form Taysurf itself were replicated upon the optic, a calibration file was taken from an optical flat to remove any of these effects.

The key to the differential deposition process is having accurate and repeatable metrology to determine the correction to be applied to the optic. Due to the iterative nature of differential deposition, each before and after measurement must be taken in the same location. To ensure repeatability while measuring the optic using the Form Talysurf, a kinematic mount was developed which would allow unique positioning of the optic relative to the profiler - as shown in Figure 3. The kinematic mount consists of 3 cylinder pairs orientated at 120° to each other that are mounted on to a y/yaw stage and 3 truncated spheres located on the optic's mount. The optic is not removed from the mount after it is initially mounted until the correction is complete, this therefore ensures accurately positioning between coatings.

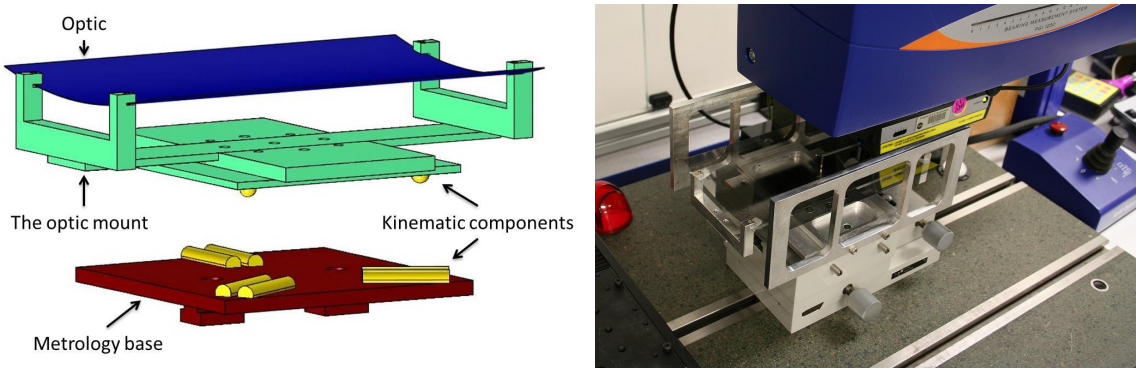

(a) (b)

Figure 3. Highlighted in 3(a) is a schematic of the kinematic mount used to ensure accurate positioning of the optic relative to the Form Talysurf stylus. 3(b) demonstrates the metrology set-up to obtain surface profiles, the y/yaw stage is clearly visible and it is on the top of this that the kinematic metrology base is fixed, which in turn mates with the kinematic component of the optical mount.

2.3 Slit profiles and correction calculation

In order to apply the correction to remove the defects on the optical surface, a mask with a slit is used to produce a well defined deposition profile. The width of the deposition profile is defined by the width of the slit which in turn is determined by the spatial frequency to be corrected. Multiple single slits with widths ranging from 3mm to 0.5mm have been studied to correct a variety of spatial frequencies (Figure 4(a)) and in order to achieve a very narrow deposition profiles to target high spatial frequency errors, a double slit approach has been also studied. In addition to changing the slit width to vary the width of the deposition profile, the distance between slit and substrate can also be varied to affect the width of the profile.

To create a deposition profile that can be used within the correction algorithm, test profiles are deposited upon a glass slide and the cross-sectional thickness at regular intervals is measured using a KLA Tencor D-100 step-profiler. Once several profiles for a given slit arrangement have been measured, the data are averaged and a set of Gaussians fitted to the data. The number and the width of the Gaussians can be varied to achieve the best fit for the measured data. The advantage of using Gaussians is that the deposition profile can be defined as a function which aids in the least squares fit of the deposition profile to the optical surface. Figure 4(b) highlights the measured deposition profile and the set of fitted Gaussians used to create the function.

A graphical user interface (GUI) has been developed to correct the Form Talysurf data with the deposition profiles functions. There are a variety of correction options available, but the general process involves selecting the area to be corrected and then determining the spacing between each function. To fit the deposition profiles

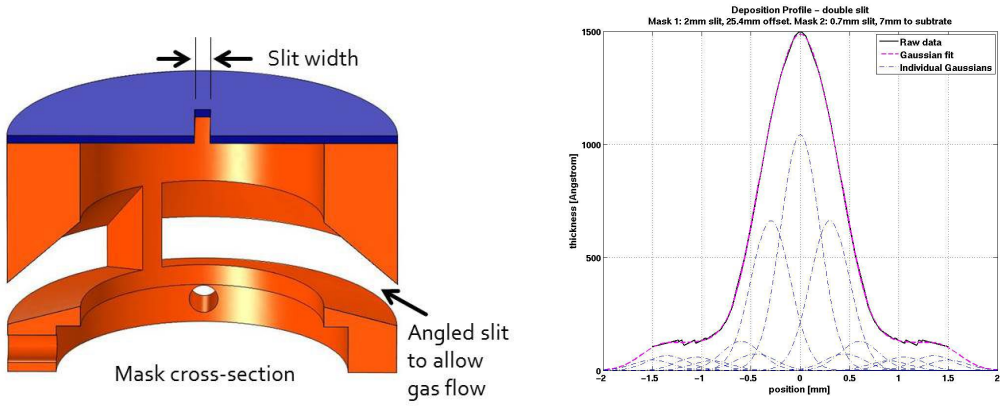

(a) (b)

Figure 4. 4(a) highlights a cross section of the mask and slit arrangement, different deposition profiles are created through varying the slit width. 4(b) demonstrates a how Gaussians are used to create a deposition profile function from thickness measurement data.

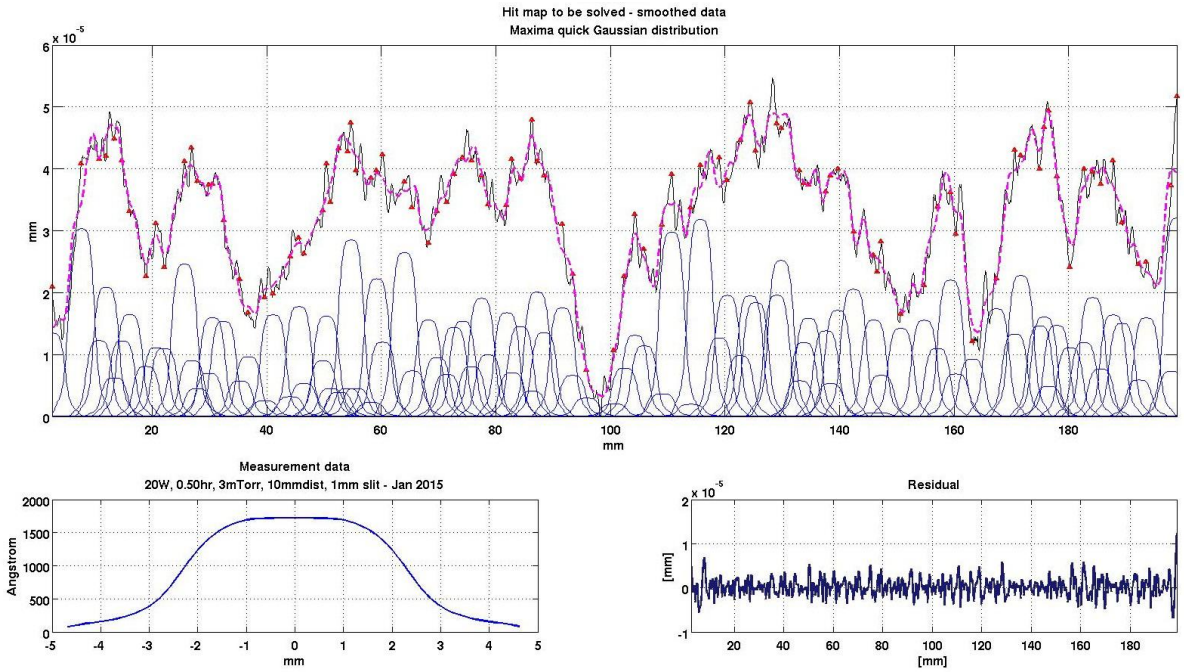

Figure 5. This figure highlights the optimisation of the metrology with the deposition profile function. The top plot depicts the profile to be corrected (solid line), the correction as determined from the sum of the deposition profile functions (dashed line) and each individual deposition profile function required for the correction (i.e. the hit-map). The bottom left plot highlights the deposition profile function and the bottom right plot demonstrates the expected residual assuming a perfect coating. This tri-plot also highlights the correction applied to Optic 1 as detailed in Section 3.1.

to the measured data a least squares fit method is used where only positive profiles are considered (i.e. a negative profile would imply removing material from the surface). Using the information from the least squares fit and the time taken while sampling the desposition profiles, a hit-map can be generated for the optical surface (Figure 5).

For current experimentation the correction process is considering a 1D single line profile; however, in the future to correct the entire surface of the optic, a 2D metrology and correction will be required.

3. INITIAL EXPERIMENTATION

This section will provide an outline of some of the inital experimentation that has been performed on the slumped glass optics provided by NASA GSFC. These optics have a Wolter I geometry and are a significant improvement upon the optics made for the NuSTAR mission.[15,16] The optics are approximately 200mm in axial length and represent a 30° sector of a full revolution optic. The radii of curvature of the initial sample optics ranged from 485mm to 494mm.

The optics were mounted within an aluminium frame work that was connected to the kinematic mount as mentioned in Section 2.2. In this initial stage of testing we were not concerned in mounting the optics with minimum distortion as only the mid to high spatial frequencies were going to be targeted. To fix the optics within the mount 4 set screws were used with Teflon shim acting as an interface between the glass and the aluminium. In order to provide a reference for the metrology relative to the optical surface, fiducials were marked upon the glass a few millimeters from the top and bottom edges.

Using the physical location of the fiducials relative to the edge of the optic and the measured location of the fiducials upon the Talysurf, the mask's slit could be aligned confidently to the optic to within ∼0.25mm. In addition, using the feedback from the encoder to the motor, the positioning is accurate to within the step size of the motor which equates to $\sim 10\mu m$.

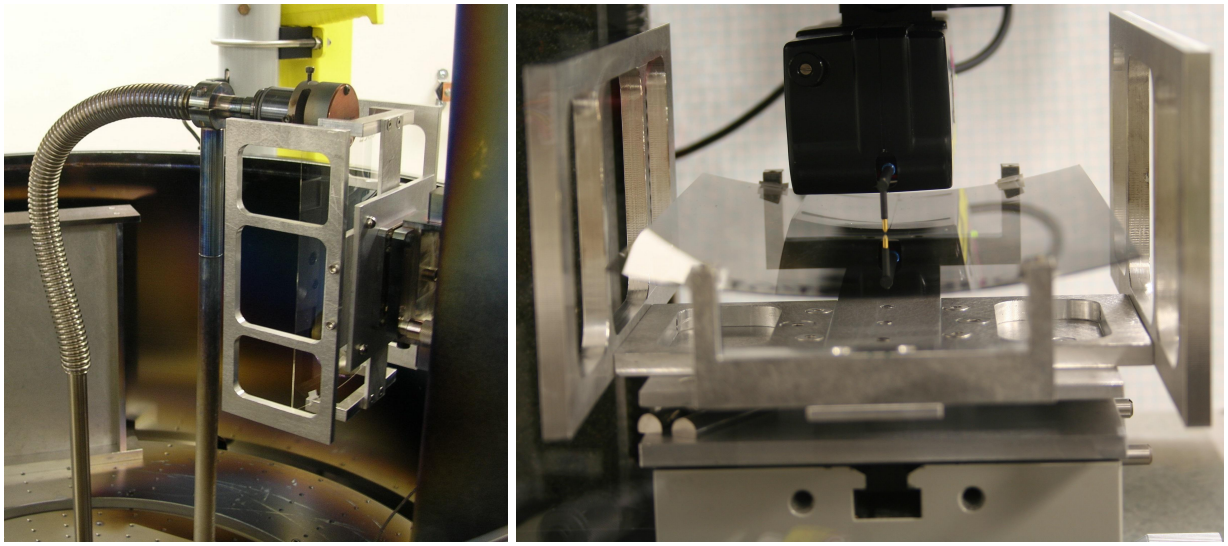

(a) (b)

Figure 6. 6(a) highlights the optic within its mount fixed upon the vertical translation stage. The mount is connected to a tip-tilt stage to aid in the alignment of the mask/magnetron head relative to the optic. Figure 6(b) demonstrates how the optic is orientated relative to the head of the Form Talysurf for profilometric measurements, in addition, two of the cylinders that form the kinemtic mount can be seen in the bottom left of the photo.

3.1 Optic 1 - 494S-6852

The metrology from the first optic showed deviations with a peak-to-valley of ∼ 500Å, because the deviations were so low in amplitude a full correction of both low and mid order spatial frequencies was performed, as shown in Figure 5. The slit width used for this initial correction was 1mm, the distance between the slit and the optical surface was positioned to 10mm and the power set to 20W. Due to time restraints, only the first 120mm of the correction was performed and the duration of the coating was approximately 2 hours 10 minutes.

The results from this first coating are shown in Figure 7. It is clear from plots that the coating was not successful in correcting the surface profile of the optic and infact, the after coating profile is much worse than the before coating profile. At this stage it was suspected that stress within the coating was the primary cause of

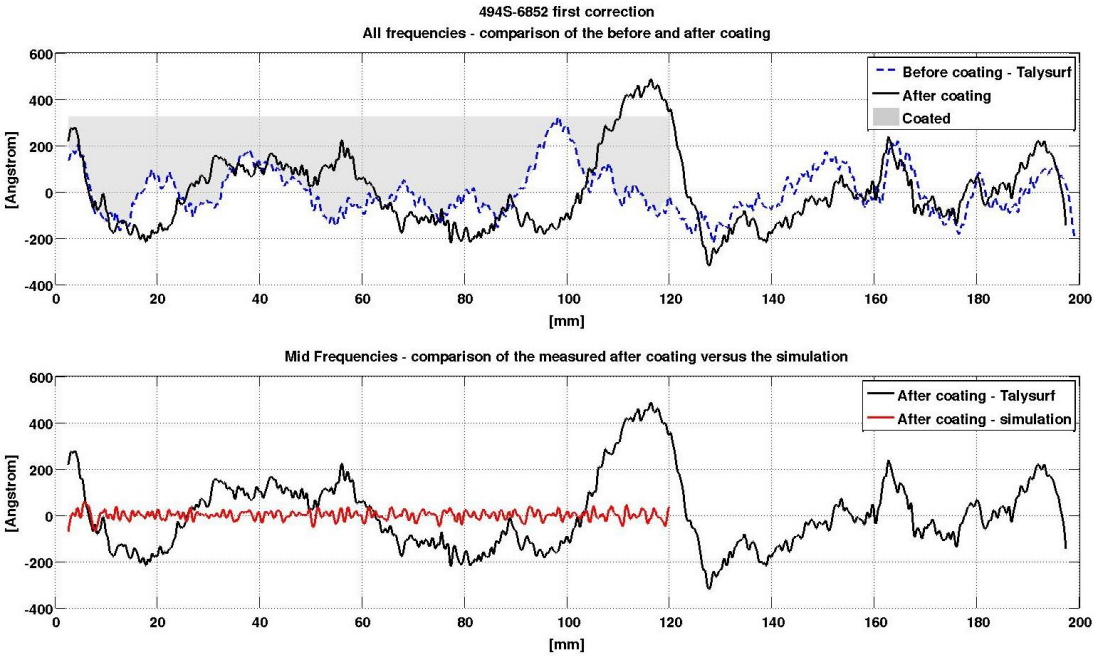

Figure 7. This graph highlights the results from the first differential deposition coating upon a slumped glass optic. The top plot highlights the before coating (dashed line), the after coating profile (solid line) and the coated region (shaded area). The bottom plots compares the measured after coating with the simulation.

deviations that were seen. It is inevitable that there will be some form of stress with the deposited thin film and despite the fact that Ni is typically a low stress metal once deposited, the low Young's modulus of glass coupled with the segmented structure of the optics could mean this low stress has a potentially large effect, especially when compared to the NiCo electroformed optics[18] which do not appear to exhibit deformations due to coating stress.

3.2 Optic 2 - 489P-2728

The profilometer data for the second optic is shown in Figure 8. From the scale on the vertical axis it can be seen that there are much larger surface deviations in the second optic when compared to the first. Following on from the lessons learnt from the first differential coating the four highlighted troughs/valleys were selected for coating, not only should the effect of stress be less but also it would provide confirmation of the positioning accuracy of the vertical translation tower and therefore overall differential deposition concept.

The spatial frequencies of the troughs to be corrected were smaller than the correction required in Optic 1 and therefore a narrower slit of 0.5mm was selected. In order to further reduce the width of the deposition profile, the distance between the slit and the optical surface was reduced to 7mm. Furthermore, to decrease the time of deposition the power was set to 30W and this led to a coating time of just under 1 hour.

The results from the first coating on Optic 2 are shown in Figure 9. The results indicate that the troughs were accurately filled in by the coating and thereby confirming the differential deposition method for the slumped glass optics. However, there is some variation between the after coating and the simulation. It is thought that this variation is due to inaccurate positioning of the optic relative to the Form Talysurf, as the kinematic mount upon the y/yaw stage had been disassembled between measurements.

Following on from this initial success, a second correction was performed on Optic 2 with the same coating philosophy. The second coating highlighted positive results and the after coating measurement and the simulation were in very close agreement. For the third coating upon Optic 2 the decision was made to be more aggressive (although still targeting localised areas), with the simulation expecting an almost flat correction.

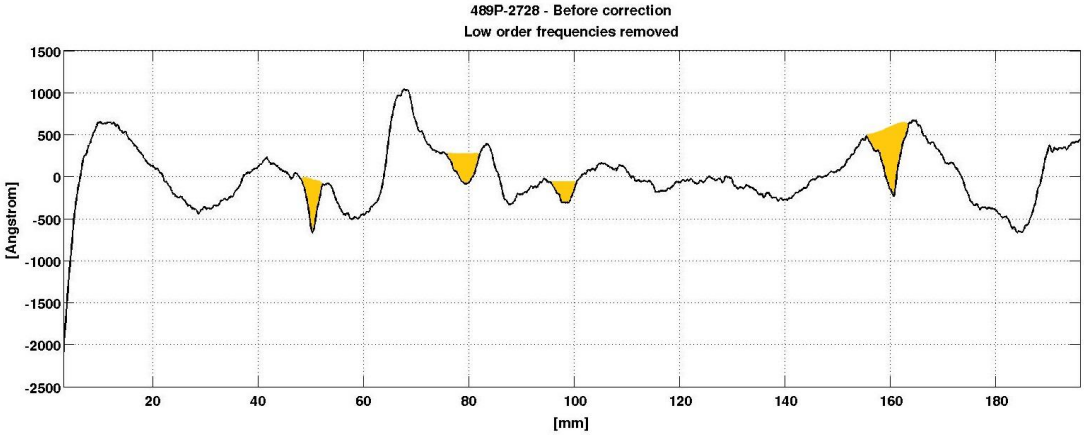

Figure 8. This plot highlights the surface profile of the second optic to be coated. The shaded regions depict the areas where the differential deposition coating would be applied

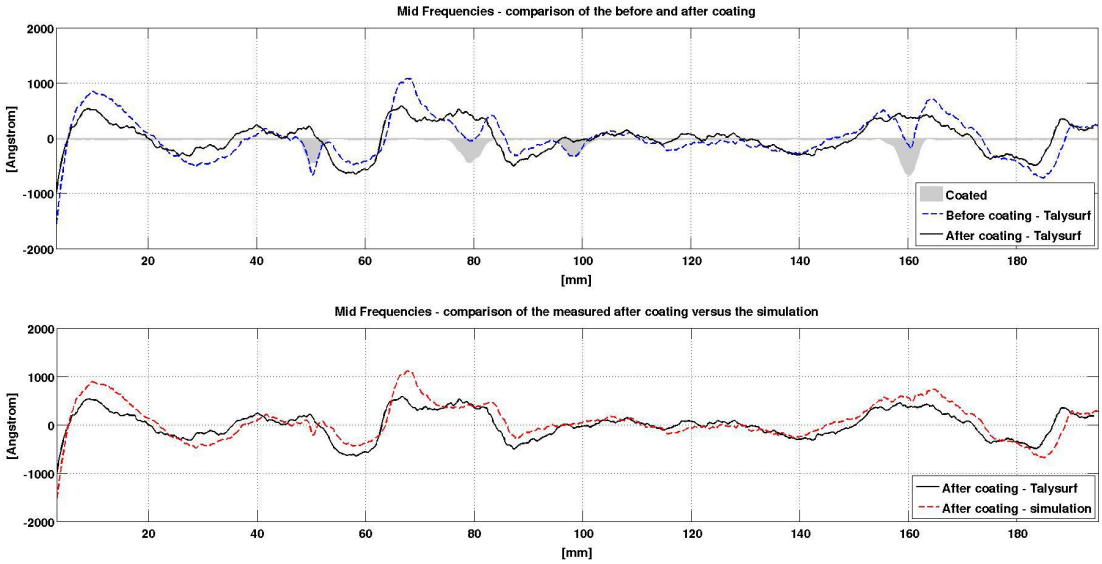

Figure 9. The top plot compares the before coating (dashed line) with the after coating (solid line) and the region of coating is shaded. In the bottom plot the after coating (solid line) is compared against the after coating simulation (dashed line).

The results from the third coating were puzzling and can be seen in Figure 10. The results indicated that the first 120mm of the optic corrected well, whereas the last 80mm became significantly worse. The cause of this error was unknown and with only one point of reference the decision was made to proceed and measure/coat Optics 3 and 4. However, the same effect became apparent on Optics 3 and 4 after one/two coatings, therefore implying that the error was inherent within the coating procedure and solving this problem became the direction of research.

4. NULL CORRECTION INVESTIGATION

With the *null correction* observed in three optics there was clearly a systematic error within some component of differential deposition procedure for the slumped glass optics. The following explanations were investigated.

1. **Stress?** - It is considered unlikely that a uniform stress within the deposit would cause the effect that

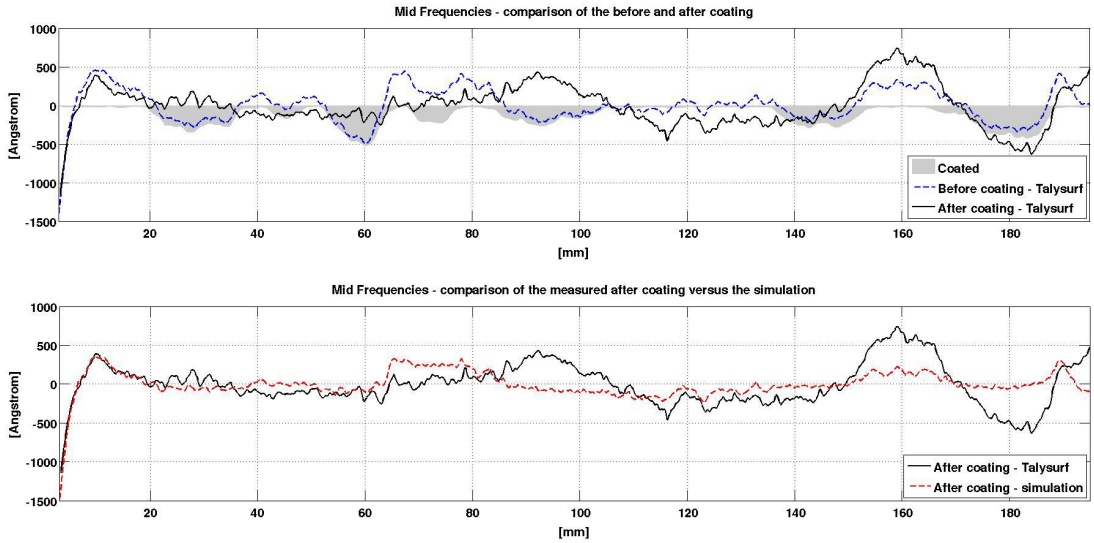

Figure 10. The top plot compares the before coating (dashed line) with the after coating (solid line) and the region of coating is shaded. In the bottom plot the after coating (solid line) is compared against the after coating simulation (dashed line).

is being seen. A uniform stress would in theory equally affect the top of the optic as well as the bottom of the optic and this is not what is observed. However, could the stress be varying with time which would potentially make coatings at the end of the deposition more stressed than those at the start? Experimentation indicated that this was not the case. A simple experiment saw only the bottom half of the optic coated and therefore it should mimic the same coating environment as at the start of the coating. The result from this test demonstrated the same deviations as seen in Optics 2-4 indicating that stress was not the primary contributor to the errors seen.

2. **Mounting?** - Is there something about the vertical mount that is causing the optic to deform while coating? For example could a gravitational distortion be altering the effect of the coating in the vertical configuration which is not seen in the horizontal metrology?

3. **Thermal effects?** - The vacuum deposition technique employed by the differential deposition correction is plasma based and known to create an increase in temperature in the immediate vicinity of the magnetron head and mask. Could the change in temperature coupled with the mismatch in CTE (coefficient of thermal expansion) between the glass optic and the aluminium mount be causing some of the distortions that are observed?

Each of these effects was investigated in turn to determine its contribution, if any, to the observed null correction, although a combination of all of these factors could also be the cause.

4.1 Stress

Although it was not suspected that stress would be the primary cause of the null correction, it was still thought to be reason why the first correction (Section 3.1) failed, therefore an estimation of the stress within the deposit was deemed worthwhile. One of the primary methods to determine stress within thin films is to use the Stoney equation[25] as shown in Equation 1, where, σ_f is the film stress, t_f is the film thickness, E_s is the substrate Young's modulus, h is the substrate thickness, ν_s is the substrate Poisson ratio and R is the radius of curvature change of the substrate after deposition.

$$\sigma_f t_f = \frac{E_s h^2}{6(1-\nu_s)R} \tag{1}$$

The Stoney calculates stress from looking at the change in radius of curvature of a substrate after coating. Therefore to estimate the stress within our deposit, four 1 inch glass wafers (Schott glass D235) were coated with a uniform thickness of nickel using the 0.5mm slit and a Talysurf measurement was taken before and after coating. A circle was then fitted to the difference between the before and after coatings and a radius of curvature for the effect of the film determined, as shown in Figure 11. Combining the stress from the four wafers an average value of 179 MPa (tensile) with a standard deviation of 53 MPa was calculated.

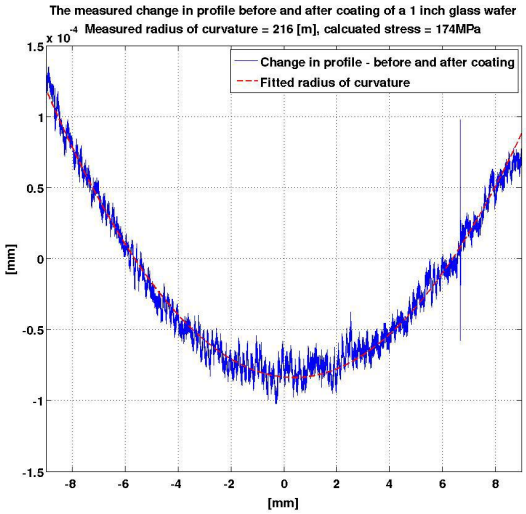

Figure 11. An example of the residual curvature from the before and after coating profilometer measurements on the 1 inch glass wafer. The fitted circle data is shown as a dashed line and in this plot the radius of curvature was calculated to be 216m, which equated to a stress value of 174MPa.

It was known prior to the experiment that there would be stress within the deposit and the value of 179 MPa is not an unrealistic as previous measurements of stress within other differential deposition deposits indicated stress in the region of 100 MPa. Knowing this value of stress there are several areas of investigation we could follow, for example the coating parameters could be changed to alter the magnitude and sign of the stress (i.e. tensile or compression) with the goal of approaching zero stress. Work to this effect has been under investigation at NASA MSFC and is highlighted in the paper by *Broadway, D. M. et al (2015)*.[26]

Another two options could be to keep the coating parameters the same and to use/incorporate the stress within the correction. The effect of the thin film stress can be modelled within finite element analysis software and therefore potentially a differential deposition correction could incorporate the effect due to stress leading to a more accurate correction. Alternatively, the stress could be used via the same method to correct the low order frequencies of the glass optic.

4.2 Mounting

In order to determine whether or not the mounting was affecting the correction, a simple experiment was devised which flipped the optic and its mount by 180°, so that the top of the optic became the bottom of the optic relative to the translation tower. The theory was that if the mount was contributing to the null correction then the error should be evident at the new bottom of the optic (0mm to 80mm).

The results are shown in Figure 12 and indicate that the mounting maybe a cause of the null correction. The coating was performed in the direction from 190mm to 0mm and although the after coating profile and the simulation profile are not in as close agreement as seen in other coatings, the results do highlight a correction

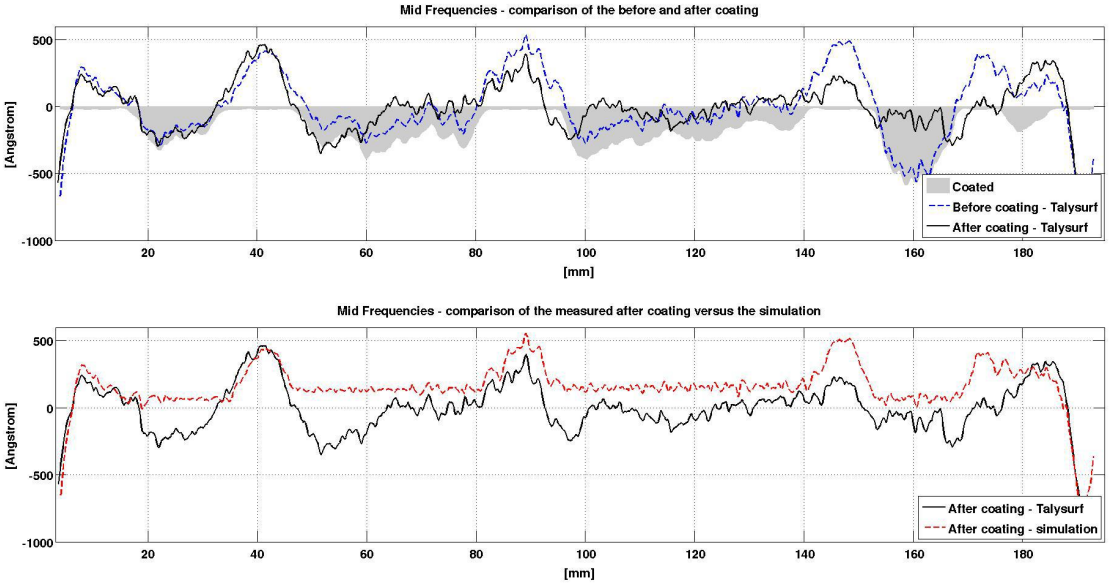

Figure 12. The top plot highlights the before (dashed blue line) coating profile, the after coating profile (solid black line) and the region where it have been coated (grey shaded region). The bottom plot shows the comparision between the after coating measured data (solid black) and the after coating simulation (red dashed line). The direction of coating was from 190mm to 0mm.

in the region from 190mm to 70mm, but then a null correction in the region from 70mm to 0mm. This result indicates that the error may lie within the structure or the material of the mount.

4.3 Temperature

The temperature within the chamber is known to increase while coating is in progress and it is also know that there is a mismatch in CTE between the glass optic[27] ($7.2 \times 10^{-6} K^{-1}$) and the aluminium mount[28] ($25.2 \times 10^{-6} K^{-1}$). Therefore in order to monitor the temperature over time, a series of K-type thermocouples were attached to both the optic and mount. Figure 13 highlights an example of temperature monitoring within the chamber, in this example a 0.5mm slit was used at 7mm from the optical surface and the slit was located in the centre of the optic. Five thermocouples were located within the chamber: one measuring the 'vacuum'/gas temperature; three located upon the glass optic and one upon the aluminium mount. The three thermocouples on the glass optic were located: immediately in front of the slit on the glass; in front of the slit on the backside of the glass; and in the bottom corner of the glass. The data collected within the figure represents 60 minutes of coating at 30W with the optic stationary relative to the slit.

The results from Figure 13 show a sharp rise in temperature in the vicinity of the slit in the first few minutes of deposition. The temperature change of the edge of the glass and the aluminium mount is more gradual over the 60 minutes, which is expected due to their distance from the source. When considering the coefficients of thermal expansion coupled with the change in temperature, it is possible that several microns of displacement is taking within place the optic.

4.4 Conclusion

From studying the stress, mounting and temperature effects within the chamber in regard to the null correction, the immediate direction of investigation as of August 2015 is towards the mount. Section 4.2 demonstrated that rotating the mount with respect to the direction of translation caused the error to shift with respect to the optic, this implied that the mounting does have an effect upon the correction. Therefore a second mount will be designed and for this second iteration the fixed points will be moved from the optic's axial edge to the azimuthal edge. The thought is that by removing the axial fixtures, the optic should be able to expand and contract more freely along the axial length without encountering fixed boundaries.

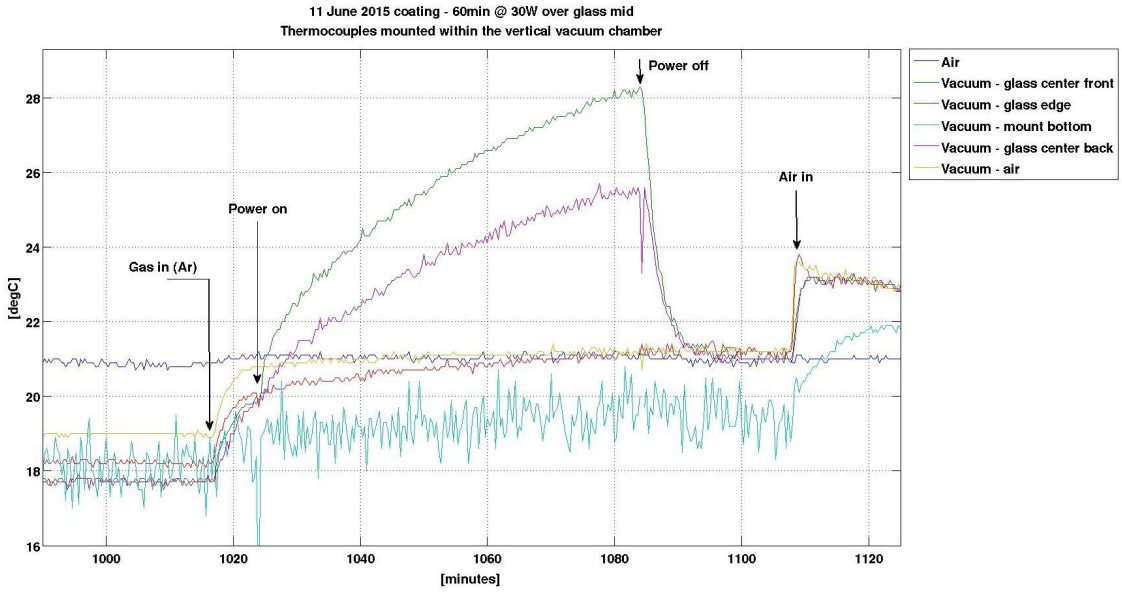

Figure 13. The thermal environment within the chamber during a 60 minute 30W coating with the optic stationary with respect to the slit.

In addition, Section 4.3 highlighted the temperature changes within the chamber during coating and the current mismatch in CTE between the optic and the mount. The obvious answer to the CTE mismatch is to change the material of the mount to have a similar CTE to that of the glass. There are many materials available with lower CTEs, such as: Invar, stainless steel and ceramic material. Invar is known for its very low CTE of $\sim 1.2 \times 10^{-6} K^{-1}$ and although stainless steel has a higher CTE of $\sim 9.4 \times 10^{-6} K^{-1}$ it is readily available and inexpensive. However, considerations of weight are important when considering that the mount will be cantilevered from a tip/tilt stage. Therefore it is proposed that the next mount to be made from a ceramic material such as Macor[29] or alumina silicate,[30] which have CTEs of $\sim 9.0 \times 10^{-6} K^{-1}$ and $\sim 3.6 \times 10^{-6} K^{-1}$ respectively. The lower density of the ceramics mean that they are lighter than their metal counterparts and therefore preferred in this instance.

Finally, it is clear from Section 4.1 that there is stress within the coating; however, it is currently not deemed the primary cause of the null correction that is observed. Therefore the effect of stress will be assessed again once the modifications to the mount have been made.

5. SUMMARY AND FUTURE WORK

The future of high resolution X-ray astronomy requires significant advances in X-ray optics technology then that which is currently available. Differential depostion upon slumped glass X-ray optics provides one solution to this requirement and presented within this paper have been the hardware, correction procedure and initial results from this effort. In comparison to the differential deposition effort on NiCo replicated optics,[18] differential deposition of thin glass shells encountered several difficulties, such as: mounting, thermal effects and stress within the deposit; however, despite these, an improvement in figure error has been demonstrated upon the glass optics.

Future research will initially be geared towards solving the null correction problem as outlined in Section 4, with the goal of achieving a repeatable and accurate correction upon the optic's surface without introducing additional figure errors. Once this has been achieved on a single axis, the investigation will look at performing differential deposition upon the entire optical surface (i.e. a 2D correction) by utilising the vertical chamber's rotation axis.

ACKNOWLEDGMENTS

The author would like to acknowledge the help from MSFC's Tribology Laboratory for the use of their metrology equipment and in addition a NASA APRA award that funded this research.

REFERENCES

[1] Weisskopf, M. C., "The Chandra X-Ray Observatory: An overview," *Advances in Space Research* **32**, 2005–2011 (2003).

[2] Jansen, F., Lumb, D., Altieri, B., Clavel, J., Ehle, M., Erd, C., Gabriel, C., Guainazzi, M., Gondoin, P., Much, R., Munoz, R., Santos, M., Schartel, N., Texier, D., and Vacanti, G., "XMM-Newton observatory. I. The spacecraft and operations," *Astronomy and Astrophysics* **365**, L1–L6 (Jan. 2001).

[3] Harrison, F. A., Craig, W. W., Christensen, F. E., Hailey, C. J., Zhang, W. W., Boggs, S. E., Stern, D., Cook, W. R., Forster, K., Giommi, P., Grefenstette, B. W., Kim, Y., Kitaguchi, T., Koglin, J. E., Madsen, K. K., Mao, P. H., Miyasaka, H., Mori, K., Perri, M., Pivovaroff, M. J., Puccetti, S., Rana, V. R., Westergaard, N. J., Willis, J., Zoglauer, A., An, H., Bachetti, M., Barrière, N. M., Bellm, E. C., Bhalerao, V., Brejnholt, N. F., Fuerst, F., Liebe, C. C., Markwardt, C. B., Nynka, M., Vogel, J. K., Walton, D. J., Wik, D. R., Alexander, D. M., Cominsky, L. R., Hornschemeier, A. E., Hornstrup, A., Kaspi, V. M., Madejski, G. M., Matt, G., Molendi, S., Smith, D. M., Tomsick, J. A., Ajello, M., Ballantyne, D. R., Baloković, M., Barret, D., Bauer, F. E., Blandford, R. D., Brandt, W. N., Brenneman, L. W., Chiang, J., Chakrabarty, D., Chenevez, J., Comastri, A., Dufour, F., Elvis, M., Fabian, A. C., Farrah, D., Fryer, C. L., Gotthelf, E. V., Grindlay, J. E., Helfand, D. J., Krivonos, R., Meier, D. L., Miller, J. M., Natalucci, L., Ogle, P., Ofek, E. O., Ptak, A., Reynolds, S. P., Rigby, J. R., Tagliaferri, G., Thorsett, S. E., Treister, E., and Urry, C. M., "The Nuclear Spectroscopic Telescope Array (NuSTAR) High energy X Ray Mission," *APJ* **770**, 103 (June 2013).

[4] Ramsey, B. D., Alexander, C. D., Apple, J. A., Benson, C. M., Dietz, K. L., Elsner, R. F., Engelhaupt, D. E., Ghosh, K. K., Kolodziejczak, J. J., O'Dell, S. L., Speegle, C. O., Swartz, D. A., and Weisskopf, M. C., "First Images from HERO, a Hard X-Ray Focusing Telescope," *APJ* **568**, 432–435 (Mar. 2002).

[5] Zhang, W. W., "Manufacture of mirror glass substrates for the NuSTAR mission," *Proc. SPIE* **7437** (Aug. 2009).

[6] Burrows, D. N., Hill, J. E., Nousek, J. A., Kennea, J. A., Wells, A., Osborne, J. P., Abbey, A. F., Beardmore, A., Mukerjee, K., Short, A. D. T., Chincarini, G., Campana, S., Citterio, O., Moretti, A., Pagani, C., Tagliaferri, G., Giommi, P., Capalbi, M., Tamburelli, F., Angelini, L., Cusumano, G., Bräuninger, H. W., Burkert, W., and Hartner, G. D., "The Swift X-Ray Telescope," *SSR* **120**, 165–195 (Oct. 2005).

[7] Gubarev, M., Ramsey, B., O'Dell, S. L., Elsner, R., Kilaru, K., McCracken, J., Pavlinsky, M., Tkachenko, A., Lapshov, I., Atkins, C., and Zavlin, V., "Development of mirror modules for the ART-XC instrument aboard the Spectrum-Roentgen-Gamma mission," in [*Society of Photo-Optical Instrumentation Engineers (SPIE) Conference Series*], *Society of Photo-Optical Instrumentation Engineers (SPIE) Conference Series* **8861**, 0 (Sept. 2013).

[8] ESA, "ATHENA - MISSION SUMMARY." http://sci.esa.int/cosmic-vision/54517-athena/.

[9] Willingale, R., Pareschi, G., Christensen, F., den Herder, J.-W., Ferreira, D., Jakobsen, A., Ackermann, M., Collon, M., and Bavdaz, M., "Science requirements and optimization of the silicon pore optics design for the Athena mirror," in [*Society of Photo-Optical Instrumentation Engineers (SPIE) Conference Series*], *Society of Photo-Optical Instrumentation Engineers (SPIE) Conference Series* **9144**, 2 (July 2014).

[10] Proserpio, L., Breunig, E., Friedrich, P., and Winter, A., "Optical design for ATHENA X-ray telescope based on slumped mirror segments," in [*Society of Photo-Optical Instrumentation Engineers (SPIE) Conference Series*], *Society of Photo-Optical Instrumentation Engineers (SPIE) Conference Series* **9144**, 5 (July 2014).

[11] Kilaru, K., Ramsey, B. D., Gubarev, M. V., and Gregory, D. A., "Differential deposition technique for figure corrections in grazing-incidence x-ray optics," *Optical Engineering* **50**(10), 106501–106501–6 (2011).

[12] Atkins, C., Wang, H., Doel, P., Brooks, D., Thompson, S., Feldman, C., Willingale, R., Button, T., Rodriguez Sanmartin, D., Zhang, D., James, A., Theobald, C., Willis, G., and Smith, A. D., "Active x-ray optics for the next generation of x-ray telescopes," in [*Society of Photo-Optical Instrumentation Engineers (SPIE) Conference Series*], **7360** (May 2009).

[13] Feldman, C., Willingale, R., Atkins, C., Wang, H., Doel, P., Brooks, D., Thompson, S., Button, T., Zhang, D., Rodriguez Sanmartin, D., James, A., Theobald, C., and Smith, A. D., "First results from the testing of the thin shell adaptive optic prototype for high angular resolution X-ray telescopes," in [*Society of Photo-Optical Instrumentation Engineers (SPIE) Conference Series*], **7437** (2009).

[14] Reid, P. B., Aldcroft, T. L., Allured, R., Cotroneo, V., Johnson-Wilke, R. L., Marquez, V., McMuldroch, S., O'Dell, S. L., Ramsey, B. D., Schwartz, D. A., Trolier-McKinstry, S. E., Vikhlinin, A. A., Wilke, R. H. T., and Zhao, R., "Development status of adjustable grazing incidence optics for 0.5 arcsecond x-ray imaging," *Proc. SPIE* **9208**, 920807–920807–9 (2014).

[15] Zhang, W. W., Biskach, M. P., Bly, V. T., Carter, J. M., Chan, K. W., Gaskin, J. A., Hong, M., Hohl, B. R., Jones, W. D., Kolodziejczak, J. J., Kolos, L. D., Mazzarella, J. R., McClelland, R. S., McKeon, K. P., Miller, T. M., O'Dell, S. L., Riveros, R. E., Saha, T. T., Schofield, M. J., Sharpe, M. V., and Smith, H. C., "Affordable and lightweight high-resolution x-ray optics for astronomical missions," *Proc. SPIE* **9144**, 15 (July 2014).

[16] Zhang, W. W., Biskach, M. P., Blake, P. N., Bly, V. T., Carter, J. M., Chan, K. W., Gaskin, J. A., Hong, M., Hohl, B. R., Jones, W. D., Kolodziejczak, J. J., Kolos, L. D., Mazzarella, J. R., McClelland, R. S., McKeon, K. P., Miller, T. M., O'Dell, S. L., Riveros, R. E., Saha, T. T., Schofield, M. J., Sharpe, M. V., and Smith, H. C., "High resolution and high throughput x-ray optics for future astronomical missions," in [*Society of Photo-Optical Instrumentation Engineers (SPIE) Conference Series*], *Society of Photo-Optical Instrumentation Engineers (SPIE) Conference Series* **8861**, 0 (Sept. 2013).

[17] Ramsey, B. D., "Replicated Nickel Optics for the Hard-X-Ray Region," *Experimental Astronomy* **20**, 85–92 (Dec. 2005).

[18] Kilaru, K., Atkins, C., Ramsey, B. D., Kolodziejczak, J. J., Lis, T. M., Gubarev, M. V., O'Dell, S. L., Gaskin, J. A., and Broadway, D. M., "Progress in differential deposition for improving the figures of full-shell astronomical grazing-incidence X-ray optics," *Proc. SPIE* **9603** (Aug. 2015).

[19] Ice, G. E., Chung, J., Tischler, J. Z., Lunt, A., and Assoufid, L., "Elliptical x-ray microscope mirrors by differential deposition," *Review of scientific instruments* **71** (July 2000).

[20] Handa, S., Mimura, H., Yumoto, H., Kimura, T., Matsuyama, S., Sano, Y., and Yamauchi, K., "Highly accurate differential depositionfor x-ray reflective optics," *Surf. Interface Anal.* **40**, 1019 – 1022 (2008).

[21] Alcock, S. G. and Cockerton, S., "A preferential coating technique for fabricating large, high quality optics," *Nuclear Instruments and Methods in Physics Research Section A* **616**, 110 – 114 (2010).

[22] Ramsey, B. D., Atkins, C., Gubarev, M. V., Kilaru, K., and O'Dell, S. L., "Optics requirements for x-ray astronomy and developments at the Marshall Space Flight Center," *Nuclear Instruments and Methods in Physics Research A* **710**, 143–150 (May 2013).

[23] Atkins, C., Ramsey, B., Kilaru, K., Gubarev, M., O'Dell, S., Elsner, R., Swartz, D., Gaskin, J., and Weisskopf, M., "X-ray optic developments at nasa's msfc," *Proc. SPIE* **8777**, 87770W–87770W–9 (2013).

[24] Civitani, M., Basso, S., Ghigo, M., Pareschi, G., Salmaso, B., Spiga, D., Tagliaferri, G., Vecchi, G., Burwitz, V., Hartner, G. D., and Menz, B., "X-ray optical units made of glass: achievements and perspectives," *Proc. SPIE* **9144**, 16 (July 2014).

[25] Janssen, G., Abdalla, M., Vankeulen, F., Pujada, B., and Vanvenrooy, B., "Celebrating the 100th anniversary of the Stoney equation for film stress: Developments from polycrystalline steel strips to single crystal silicon wafers," *Thin Solid Films* **517**, 1858–1867 (Jan. 2009).

[26] Broadway, D. M., Weimer, J., Gurgew, D., Lis, T., Ramsey, B. D., O'Dell, S. L., Gubarev, M., Ames, A., and Bruni, R., "Achieving zero stress in iridium, chromium, and nickel thin films," *Proc. SPIE* **9510** (May 2015).

[27] SchottNorthAmericaInc., "D 263 M Glass for Microscopy Cover Slips," tech. rep. (May 2013).

[28] MatWeb.com, "Data sheet - Aluminum 6061-T6; 6061-T651." http://www.matweb.com/.

[29] TechincalProductsInc., "Macor (MGC) Material Specifications." http://www.technicalproductsinc.com/pdf/Macor

[30] TechincalProductsInc., "Alumina Silicate Grade A Lava Material Specifications." http://www.technicalproductsinc.com/pdf/Lava.pdf.